3D-Stacked 1Megapixel Dual-Time-Gated Color SPAD Image Sensor with Simultaneous Dual Image Output Architecture for Efficient Sensor Fusion

K. Chida, K. Morimoto, N. Isoda, H. Sekine, T. Sasago, Y. Maehashi, S. Mikajiri, K. Tojima, M. Shinohara, A. Abdelghafar, H. Tsuchiya, K. Inoue, S. Omodani, A. Ehara, J. Iwata, T. Itano, Y. Matsuno, K. Sakurai, and T. Ichikawa

Canon Inc., Kanagawa, Japan,
TEL: +81-3-3758-2111
E-mail: chida.kazuma@mail.canon

Abstract—We present a 5μm-pitch, 3D-BSI 1Megapixel dual-time-gated color SPAD image sensor enabling a simultaneous output of dual images. The developed SPAD image sensor is verified to operate as an RGB-D sensor without complex image alignment. In addition, a novel HDR technique, utilizing pileup effect with two parallel in-pixel memories, is validated for dynamic range extension in 2D imaging, achieving a dynamic range of 119.5dB. The proposed architecture provides dual image output with the same field-of-view, resolution, and frame timing, and is promising for efficient sensor fusion.

I. INTRODUCTION

Sensor fusion is crucial in numerous applications, including automotive, AR/VR, mobile phones, and machine vision applications. Integrating data from multiple sensors with different field-of-view, resolution, and frame timing poses substantial computational overhead. To overcome this challenge, researchers have developed multi-functional sensors capable of operating with a monocular configuration.

One of the major topics of the sensor fusion is RGB-Depth (RGB-D) imaging. Commercially available systems have utilized a combination of an RGB camera and a time-of-flight (ToF) camera. This approach requires complex post-processing to generate RGB-D images. Additionally, differences in the field-of-view between the two cameras can cause occlusion artifacts. To address these challenges, researchers have proposed a monolithic sensor integrating RGB and ToF (NIR) pixels within the same focal plane [1], a method that alternately captures RGB and ToF images [2]. Despite these advancements, image alignment process is still required due to differences in resolution and frame timing. Furthermore, these approaches reduce spatial or temporal fill factor for RGB and ToF images, and limit signal-to-noise ratio (SNR) and depth precision.

Another important topic is the dynamic range extension in 2D imaging. High dynamic range (HDR) 2D imaging typically requires combining multiple images of different exposure time captured at different frame timing, and aligning them. To ensure the same frame timing, one applicable technique is to utilize multiple parallel in-pixel memories in CMOS [3] and SPAD [4] image sensors. Yet, further improvements in HDR performance are still needed.

Recently, time-gated SPAD image sensors have enabled multiple sensing modalities including 2D imaging and 3D ToF sensing [5-9] with a monocular configuration. Furthermore, dual-time-gated SPAD image sensor capable of streaming two independent images has been developed [9]. However, relevant applications of the dual-time-gated SPAD image sensor with 250kpixel and 16.38μm pitch have been mostly limited to bio-imaging and spectroscopy [9,10].

In this paper, we present a 5μm-pitch, 3D-BSI 1Megapixel dual-time-gated color SPAD image sensor enabling a simultaneous output of dual images for efficient sensor fusion. This sensor is verified to operate as an RGB-D sensor without complex image alignment. In addition, a novel HDR technique utilizing pileup effect is demonstrated for dynamic range extension in 2D imaging. The dual images are captured simultaneously from a single sensor, and these images have the same field-of-view, resolution, and frame timing.

II. ARCHITECTURE & OPERATIONS

Fig. 1 depicts the sensor block diagram and timing diagram. A pixel array consists of a 1,020×1,020 3D-BSI charge focusing SPAD array, with each photodiode connected to a pixel circuit. Dual gate windows can be controlled by recharge and gating pulses (Φ_R, Φ_G and Φ_{G2}), distributed through two sets of binary trees. The pixel array outputs a stream of 1-bit frames to two sets of DFE/MIPI blocks, which are summed to 4-bit frame at a SRAM frame memory for efficient data compression. 4-bit frames are then transferred to an external FPGA via MIPI interface at 1,310fps. The successive 4-bit frames are further aggregated to a higher bit depth frame, e.g. 8-bit frame. FPGA generates synchronized trigger pulses for laser emission, Φ_R, Φ_G and Φ_{G2}, with the rise and fall edge timings individually adjustable to a resolution of 100ps.

Fig. 2 shows a pixel circuit architecture and timing diagram. Each pixel has two parallel 1-bit memories. For each pixel, Φ_R and Φ_G define gate window 1 for P_OUT_1, while Φ_R and Φ_{G2} define gate window 2 for P_OUT_2. This dual-time-gated SPAD sensor can be operated in conventional dual recharge mode and proposed single recharge mode. In dual recharge mode, second recharge operation is performed between gate window 1 and gate window 2, and each gate window is independently defined. Therefore, any photons are simply detected within each gate window. In contrast, in single recharge mode, photon detection in gate window 1 disables subsequent gate window 2 via control latch, and no photons will be detected in gate window 2 until the next recharge operation. As shown in pixel timing diagrams, under high-light conditions, single recharge mode reduces the probability of photon detection in gate window 2.

III. MEASUREMENT RESULTS

Fig. 3 illustrates a timing chart for RGB-D operation in dual recharge mode, and expected photon count distribution as a function of gate position. In RGB-D operation, gate window 1 and gate window 2 are shifted with respect to laser pulse emission. The 3D ToF image is reconstructed from multiple 2D images capturd with shifted gate window 1. The distance from the camera to the target is estimated by the peak detection of the photon count histogram. The multi-bit 2D RGB image is obtained by accumulating 2D images captured with gate window 2.

Fig. 4 shows measured 3D images, 2D RGB images, and reconstructed point clouds under high-depth-precision and high-frame-rate operations. The 3D ToF image and the 2D RGB image were captured with full resolution at same field-of-view and frame timing, thereby simplifying the reconstruction process of point clouds. The 3D ToF images were reconstructed using peak detection with curve fitting. By adjusting the number of accumulated frames, the range of gate shift, and the gate shift step, various operations can be performed. In high-depth-precision operation, the RGB-D image was obtained at a frame rate of 0.45fps, suited for 3D scanning of stationary objects using 8-bit frames with shifted gate windows. The dual gate windows are shifted with respect to the laser trigger by steps of 100ps over a range of 18ns. In contrast, the high-frame-rate RGB-D image was captured at a frame rate of 36.51fps, appropriate for moving objects, using 4-bit frames shifted by 500ps steps over the same range. Despite the reduced depth precision, the reconstructed point cloud is still reliable for some tasks such as object detection.

Fig. 5 illustrates timing charts for HDR operation in single and dual recharge modes, the measured and fitted output photon counts, and the equations of the photon response curve. The timing charts show the sequences in 1-bit frame, where τ_1 and τ_2 represent the durations of gate window 1 and gate window 2, respectively. The number of Φ_R-Φ_G pairs and Φ_R-Φ_{G2} pairs per 1-bit frame are denoted by k_1 and k_2. $N_{out1}^{S,D}$, N_{out2}^{S} and N_{out2}^{D} represent the theoretical output counts for gate window 1, gate window 2 in single recharge mode, and gate window 2 in dual recharge mode. In this experiment, the ratio between τ_1 and τ_2 is set to 1:10, and then the fitted values of k_1 and k_2 are 6.4 and 6.2. The fitted curves are in good agreement with the measured output counts. In single recharge mode, the photon response curve at gate window 2 decreases under high-light conditions due to the effect of the control latch, and it enables a dynamic range extension. A dynamic range of 100.4dB is measured in dual recharge mode, and 119.5dB in single recharge mode.

Fig. 6 shows measured 10-bit images at each gate window, the incident photon count maps, HDR images in dual and single recharge modes, and its reconstruction flow. As shown in the 10-bit images, generated by summing up 4-bit frames, images captured with gate window 1 are almost identical in both modes. In contrast, areas that saturated in dual recharge mode exhibit as lower output count values in single recharge mode. The incident photon count map can be generated using a lookup table based on the output photon counts for each gate window. In both modes, low-light (red) and mid-light (green) regimes are almost the same, while a gray level for high-light regime (blue) can be represented exclusively in single recharge mode. The HDR image, reconstructed by the incident photon count map, indicates that some parts of the scene are overexposed in dual recharge mode, while the scene is clearly visible and the color is recognized in single recharge mode. Fig. 7 shows the state-of-the-art comparison for time-gated SPAD image sensors.

IV. CONCLUSION

In this paper, a 5μm-pitch, 3D-BSI 1Megapixel dual-time-gated color SPAD image sensor is presented. The sensor can simultaneouslly capture individual dual images, which have the same field-of-view, resolution, and frame timing. This work demonstrates one of the smallest pitches and the largest array sizes, while achieving best-in-class gating performance in terms of the minimum gate length, and gate skew. The proposed sensor is verified to operate as an RGB-D sensor. In addition, a newly proposed HDR technique, utilizing pileup effect with two parallel in-pixel memories, is validated for dynamic range extension in 2D imaging. The developed SPAD image sensor allows efficient sensor fusion without requiring image alignment for numerous imaging and sensing applications.

V. REFERENCES

[1] W. Kim *et al*., "A 1.5Mpixel RGBZ CMOS image sensor for simultaneous color and range image capture," *IEEE International Solid-State Circuits Conference*, 392-394, 2012.

[2] S. -J. Kim *et al*., "A 640×480 image sensor with unified pixel architecture for 2D/3D imaging in 0.11μm CMOS," *Symposium on VLSI Circuits - Digest of Technical Papers*, 92-93, 2011.

[3] A. Tournier *et al*., "A HDR 98dB 3.2μm Charge Domain Global Shutter CMOS Image Sensor," *IEEE International Electron Devices Meeting*, 10.4.1-10.4.4, 2018.

[4] N. A. W. Dutton *et al*., "High dynamic range imaging at the quantum limit with single photon avalanche diode-based image sensors," *Sensors*, 18 (4) 1166, 2018.

[5] K. Morimoto *et al*., "Megapixel time-gated SPAD image sensor for 2D and 3D imaging applications," *Optica*, 7 (4) 346-354, 2020.

[6] M. Perenzoni *et al*., "A 160×120 Pixel Analog-Counting Single-Photon Imager With Time-Gating and Self-Referenced Column-Parallel A/D Conversion for Fluorescence Lifetime Imaging," *IEEE Journal of Solid-State Circuits*, 51 (1) 155-167, 2016.

[7] I. Gyongy *et al*., "A 256×256, 100-kfps, 61% Fill-Factor SPAD Image Sensor for Time-Resolved Microscopy Applications," *IEEE Transactions on Electron Devices*, 65 (2) 547-554, 2018.

[8] K. Morimoto *et al*., "3D-Stacked 1Megapixel Time-Gated SPAD Image Sensor with 2D Interactive Gating Network for Image Alignment-Free Sensor Fusion," *IEEE Symposium on VLSI Technology and Circuits*, 1-2, 2024.

[9] M. Wayne *et al*., "A 500×500 Dual-Gate SPAD Imager With 100% Temporal Aperture and 1 ns Minimum Gate Length for FLIM and Phasor Imaging Applications," *IEEE Transactions on Electron Devices*, 69 (6) 2865-2872, 2022.

[10] M. A. Wayne *et al*., "Massively parallel, real-time multispeckle diffuse correlation spectroscopy using a 500×500 SPAD camera," *Biomedical Optics Express*, 14 (2) 703-713, 2023.

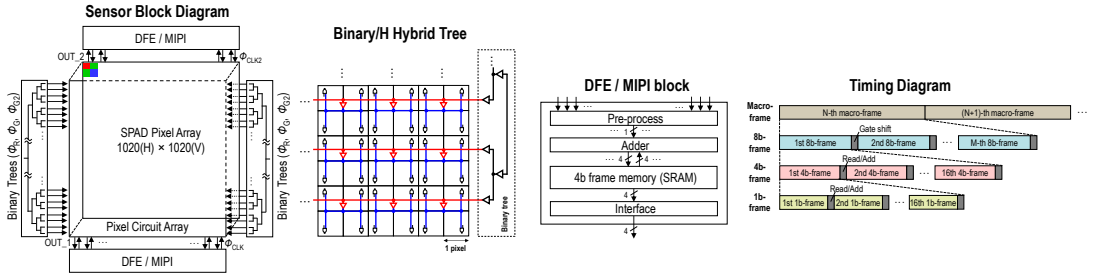

Fig. 1 Sensor block diagram, clock tree configuration, and timing diagram.

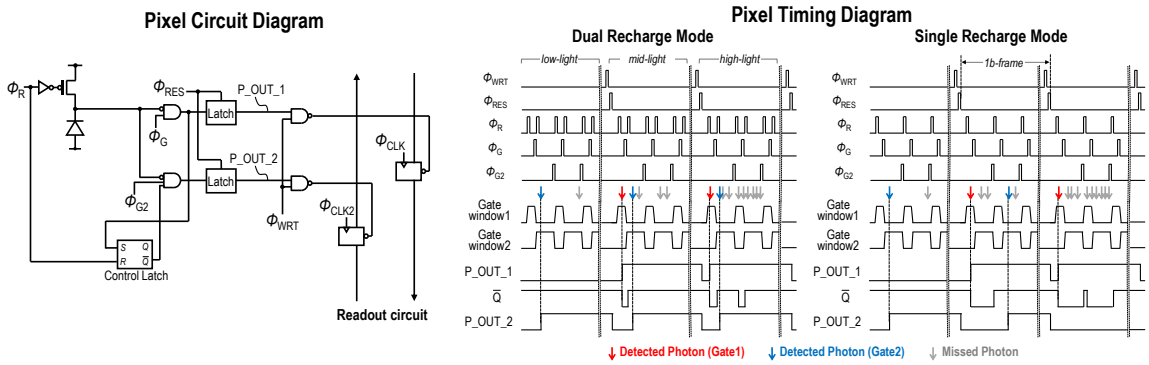

Fig. 2 Schematics of pixel circuit, and pixel timing diagrams in dual and single recharge modes.

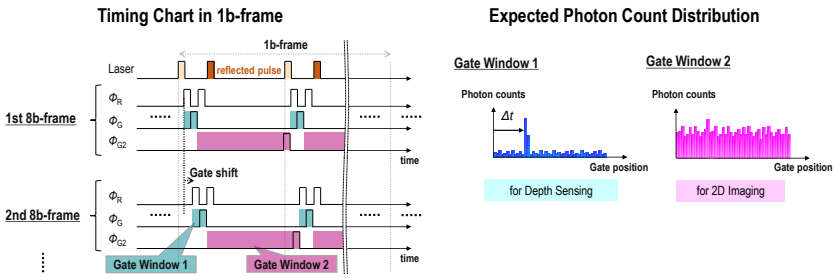

Fig. 3 Timing chart for pixel circuit in RGB-D operation, and expected photon count distribution.

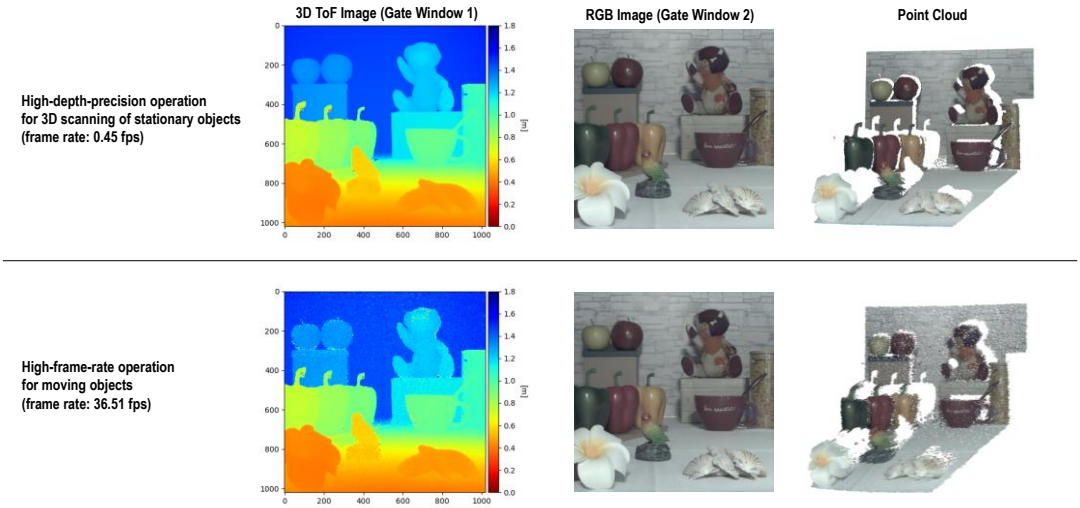

Fig. 4 Measured RGB-D images and point clouds under high-depth-precision (top) and high-frame-rate operations (bottom). (3D image and RGB image are reconstructed by gate 1 images and gate 2 images, respectively.)

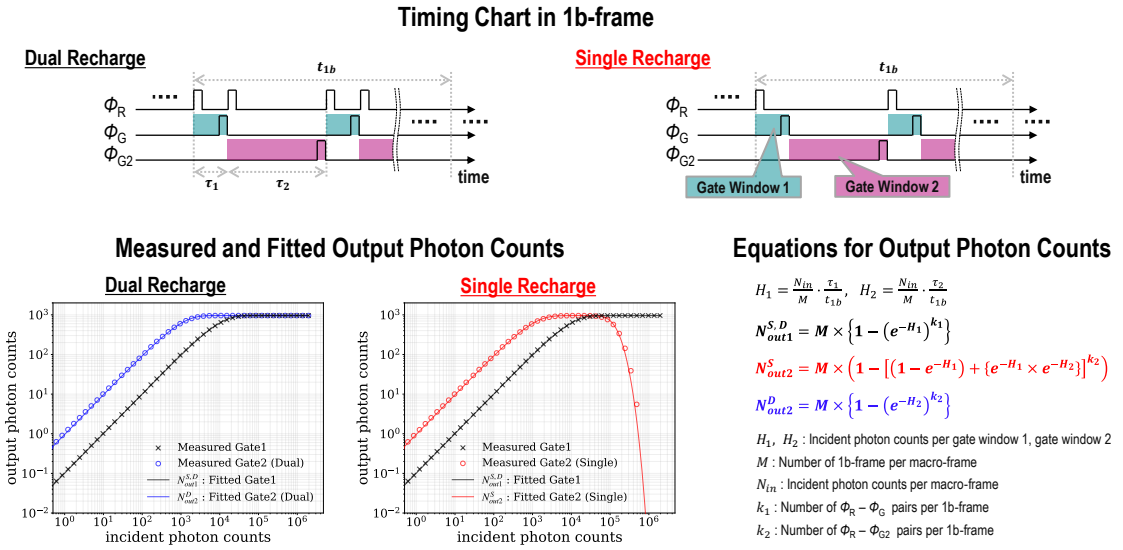

Fig. 5 Timing chart for HDR operation in dual and single recharge modes, measured (markers) and fitted (solidlines) output photon counts as a function of incident photon counts, and the equations of the photon response curve.

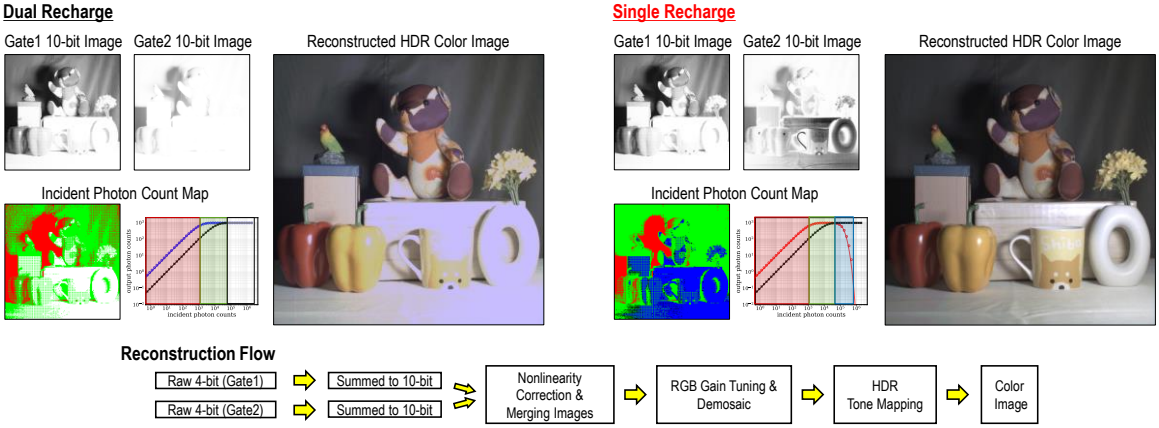

Fig. 6 Measured images at each gate window, HDR color images in dual and single recharge modes, incident photon count map, and its reconstruction flow.

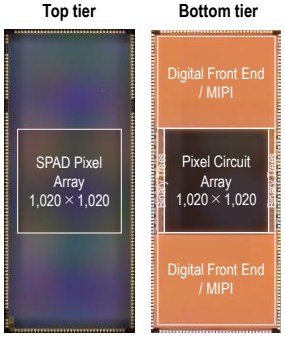

	Perenzoni (2016) [6]	Gyongy (2018) [7]	Morimoto (2020) [5]	Wayne (2022) [9]	Morimoto (2024) [8]	**This work (Gate1 / Gate2)**
Process technology	350nm HV CMOS	130nm CIS	180nm CMOS	180nm CMOS	90nm/55nm 3D-BSI CMOS	**90nm/55nm 3D-BSI CMOS**
Die size (mm × mm)	3.42 × 3.55	5 × 5	11 × 11	9.6 × 9.7	6.3 × 10.9	**6.3 × 14.8**
Sensor resolution	160 × 120	256 × 256	1,024 × 1,000	500 × 500	1,020 × 1,020	**1,020 × 1,020**
Pixel pitch (μm)	15	16	9.4	16.38	5	**5**
Exposure modes	GS	RS / GS	RS / GS	RS	Seamless GS	**Seamless GS**
Frame rate (fps)	486 (5.4b)	100,000 (1b)	24,000 (1b)	49,800 (1b × 2)	1,310 (4b)	**1,310 (4b × 2)**
Fill factor (%)	21	61	7	10.5	~100	**~100**
PDE at 940nm (%)	N/A	N/A	<0.5	N/A	23	**23**
Min. gate length (ns)	0.75	4.0	3.8	1.0	1.85	**1.60 / 1.70**
Gate length variation (ps)	80.2 (std. dev.) 189 (FWHM)*1	N/A	120 (FWHM)	70 (std. dev.) 165 (FWHM)*1	125 (FWHM)	**135 / 118 (FWHM)**
Gate skew (ps)	N/A	N/A	410 (FWHM)	109.4 (FWHM)	80 (FWHM)	**94 / 119 (FWHM)**
Power consumption at saturation (mW)	N/A	N/A	18,236 (per 1Mpixel)	N/A	505	**1053**
Pixel output bit depth	5.4b (analog)	1b	1b	1b × 2channels	4b	**4b × 2channels**
Mono/Color	Monochrome	Monochrome	Monochrome	Monochrome	Monochrome	**Color**

*1 Standard deviation (σ) converted to FWHM by: FWHM $= 2\sigma\sqrt{2\log 2}$

Fig. 7 Chip micrographs, and state-of-the-art comparison table for time-gated SPAD image sensors.